

# Flexural behaviour of steel plate-masonry composite beams

Deng-Hu Jing<sup>\*1</sup>, Shuang-Yin Cao<sup>1</sup> and Lei Shi<sup>2</sup>

<sup>1</sup>*School of Civil Engineering, Southeast University, Nanjing, Jiangsu, 210096, China*

<sup>2</sup>*Green Town Architecture Design Co., Ltd., Hangzhou, Zhejiang, 310013, China*

*(Received October 02, 2010, Revised March 10, 2012, Accepted May 01, 2012)*

**Abstract.** Steel plate-masonry composite structure is a newly-developed type of structural technique applicable to existing masonry buildings by which the load-bearing walls can be removed for large spaces. This kind of structure has been used in practice for its several advantages, but experimental investigation on its elements is nearly unavailable in existing literature. This paper presents an experimental study on the flexural behaviour of four steel plate-masonry composite beams loaded by four-point bending. Test results indicate that failure of the tested beams always starts from the local buckling of steel plate, and that the tested beams can satisfy the requirement of service limit state. In addition, the assumption of plane section is still remained for steel plate prior to local buckling or steel yielding. By comparative analyses, it was also verified that the working performance of the beam is influenced by the cross-section of steel plate, which can be efficiently enhanced by epoxy adhesive rather than cement mortar or nothing at all. Besides, it was also found that the contribution of the encased masonry to the flexural capacity of the composite beam cannot be ignored when the beam is injected with epoxy adhesive.

**Keywords:** steel plate; injection material; composite beam; local buckling.

---

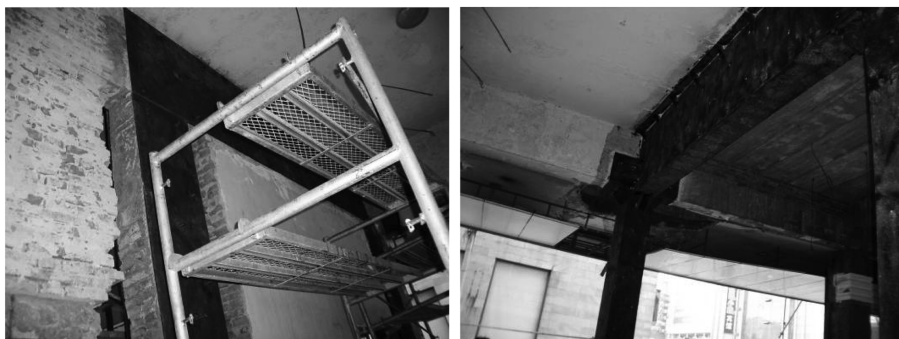
## 1. Introduction

Steel plate-masonry composite structure, composed of external steel plate, encased masonry, pressure-injected bonding material such as epoxy adhesive or cement grout, and binding bolts, is characterized by an innovative structural concept as it takes a full advantage of the mechanical behaviour of its two main components of steel plate and masonry. On one hand, the local critical buckling stress of steel plate can be efficiently enhanced due to restriction of binding bolts, rigid support of interior masonry, and even the bonding stress from the injection material (assuming that the material can provide good bond force); on the other hand, the compressive strength of encased masonry also plays a role in the compression zone of the cross section. This type of composite structure is highly applicable to existing masonry structure buildings where some load-bearing walls are to be removed for large spaces. In such buildings, the load transfer path is obviously changed because of the removal of walls, so it is necessary to introduce a new effective load-transfer system containing beams and columns so as to ensure the safety of the entire structure. Generally, steel plates are welded into rectangular, L-shaped or T-shaped cross-sections for columns, and into U-shaped cross-section for

\* Corresponding author, Associate Professor, Ph.D., E-mail: [jingdh@seu.edu.cn](mailto:jingdh@seu.edu.cn)

beams. These columns and beams can form a steel plate-masonry composite frame to bear the load instead of the original walls. In conventional technology, to realize the load-transfer, a couple of reinforced concrete beams are made to clamp the masonry wall on its both sides, or a single beam is produced to embed the wall. By comparison, the new technique has a number of advantages: (1) it shortens construction time, and requires neither wet work nor formwork, since the steel plate-masonry composite elements do not need concrete; (2) bolting and welding are relatively simple construction procedure; and (3) steel plates only cause a small dimensional increase of the beam. However, it should be noticed that whether using the above technique or the conventional approach, the method for reinforcing foundation of the building is the same. In addition, the masonry discussed in this paper only refers to solid brick masonry unless otherwise specified.

The components of a steel plate-masonry composite frame, i.e., beams and columns, are mainly manufactured from the existing masonry wall by the following steps: (1) Remove the plaster coating on both surfaces of the masonry walls where a beam and/or a column need be added, then clear the surface dust and replace it with cement mortar of 5 to 10 mm thickness (the compressive strength of the cement mortar should not be lower than 5.0 MPa for practical reason). (2) Cut 3 mm × 3 mm (width and depth) orthogonal grooves at a center-to-center spacing of 150 mm, with an angle of 45° to the axis of the beam or column in the cement mortar before it hardens into a mass. (3) Fix the pre-manufactured steel plates on the walls by binding the bolts and welding the nuts to prevent screws from loosening. (4) Remove the partial walls near the composite column (Fig. 1(a)), and weld additional steel plates onto the remaining sides of the column to form a closed region. If necessary, use cement mortar to fill the holes in the encased masonry of the composite column, since the masonry cannot always be removed precisely along the sides of the column. (5) Inject the bonding material into the composite columns through the holes drilled in the steel plates, to fill all the gaps between the steel plates and the internal masonry, as well as those among the connecting joints in the encased bricks. (6) After about 24 hours, during which time the injection material could harden into a mass, remove the partial walls beneath the composite beam and weld additional steel plates on the bottom of the beam. However, it is suggested that the composite beam with a span larger than 5 m be built in segmental progress by removing the walls and welding the steel plates gradually from its middle to both ends. This method helps avoid an unacceptable bending moment before the composite beam is completely fabricated. Otherwise, special safety measures should be provided during the entire construction period. (7) Weld the steel plates together at beam-column joints to establish an effective beam-column connection for moment resistance (Fig. 1(b)). (8) Inject the bond material into the composite beam following the same way as



(a) Removal of partial walls near the column      (b) Establishment of composite beam and columns

Fig. 1 Steel plate-masonry composite structure applied to an existing masonry building

the composite column. (9) Apply rust prevention and fire resistance coating on the surface of the steel plates for a long service life. In addition, welding should be performed prior to injecting epoxy adhesive in order to prevent the adverse influence of high temperature on the behaviour of epoxy adhesive.

Over the past decades, different combinations of steel and masonry have been widely used. To date, a lot of researchers have been doing research on this subject, but the majority of them concentrated on steel frames with infilling masonry (Moghaddam 2004, Perera *et al.* 2004), arching action between steel lintel and masonry wall (Hardy *et al.* 1995, Hardy 2000), masonry walls reinforced with steel plates (Galano *et al.* 1998, Taghdi *et al.* 2000), masonry arches strengthened with steel plates (Borri *et al.* 2009), and brick masonry confined by inlaid steel plates (Ewing *et al.* 2004). However, experimental studies on the steel plate-masonry composite elements are rather limited, in spite of the fact that steel plate-masonry composite structure has been successfully used to obtain large spaces in existing masonry buildings in China (Jing *et al.* 2009). Against the above background, it is essential to further investigate the behaviour of this type of composite members. Therefore, a total of four steel plate-masonry composite beams were tested to study their working mechanism and failure modes.

## 2. Experimental programme

### 2.1 Beam construction

To investigate the behaviour of the composite beam mentioned above, all the four specimens were made from walls of a masonry building, which was built in China in the early 1980s. Fig. 2 and Fig.3 show the details of these composite beams. As shown in Fig. 3, beam L1 was a combination of one piece of the wall and two side steel plates fixed by binding bolts, without bottom plate and injection bond material. It was designed to simulate the special period when the wall was removed before installing the bottom plate to the beam. All the bolts were 14 mm-diameter steel threaded rods. The water/cement ratio of cement grout was 0.6-0.8 (Portland cement 32.5), and the tensile strength of epoxy adhesive was 32 MPa according to the manufacturer's instruction. Besides, binding bolt spacing

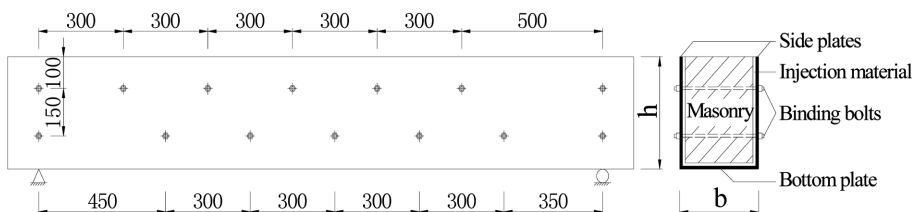


Fig. 2 Details of Beam

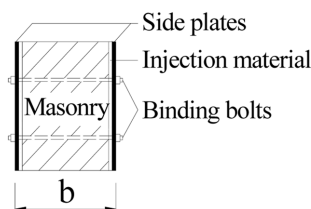


Fig. 3 Cross-section of beam L1

Table 1 Dimensions and injection materials of beams

Beam	Section width, $b$ (mm)	Section height, $h$ (mm)	Length of beam (mm)	Thickness of bottom plate (mm)	Thickness of side plate (mm)	Injection material
L1	248	352	2220	No plate	5.6	No material
L2	243	355	2170	5.6	5.6	Cement grout
L3	245	355	2220	5.6	5.6	Epoxy adhesive
L4	250	355	2180	9.4	7.3	Epoxy adhesive

was determined on the basis of existing practical practices.

For all the composite beams tested, the total width of the cross-section (i.e.,  $b$ ) is the sum of the width of the existing wall and two times the thickness of the side plate; the height, (i.e.,  $h$ ) was 350 mm. The total length of the beam was 2,200 mm, with a clear span of 2,000 mm between two supporting points. The dimensions of all specimens and the injection materials are listed in Table 1.

## 2.2 Component material properties

The thicknesses of the steel plates used in this study include: 5.6, 7.3, and 9.4 mm. The mechanical properties of the steel plate, binding bolt, and encased masonry with injection material were determined by the tensile or compressive testing, with the test data shown in Table 2.

## 2.3 Instrumentation

For the purpose of investigating the flexural behaviour of steel plate-masonry composite beam, the beams were carefully instrumented to obtain the required data at different load levels. A linear variable differential transformer (LVDT) was used to monitor the mid-span deflection of each beam; meanwhile, two dial test indicators were fixed at both beam-supporters to record support settlement. Numerous

Table 2 Material properties of components

Material		Properties (MPa)	Value
Steel plate	For 5.6 mm	Yield strength	308.7
		Ultimate strength	443.7
		Elastic modulus	206000
	For 7.3 mm	Yield strength	264.8
		Ultimate strength	404.9
		Elastic modulus	206000
	For 9.4 mm	Yield strength	274.0
		Ultimate strength	416.6
		Elastic modulus	206000
Binding bolt	Yield strength	401.6	
	Ultimate strength	526.1	
	Elastic modulus	210000	
Masonry	Injection cement grout	Compressive strength	2.13
	Injection epoxy adhesive	Compressive strength	3.13

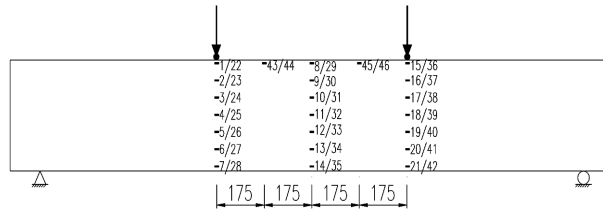


Fig. 4 The locations of strain gauges in beam L1 (front/back side)

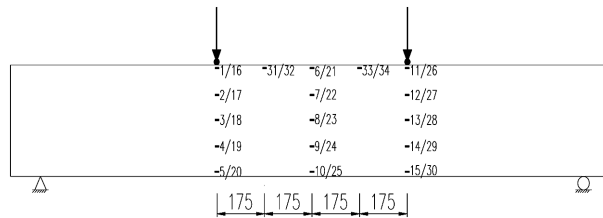


Fig. 5 The locations of strain gauges in beam L3 (front/back side)

strain gauges were bonded to the steel plate surface to monitor strain development. The locations of all the strain gauges in beams L1 and L3 are shown in Fig. 4 and Fig. 5, with the other two beams (L2 and L4) having a strain gauge arrangement similar to beam L3. The distribution of strain gauges along the depth of the beam had two types: one with five gauges located uniformly distributed at five equally spaced points, the other with seven gauges at seven points in a similar fashion. The readings of the strain gauges, LVDT, and load cells, were scanned and recorded automatically within a data-acquisition system. Fig. 6 shows the test setup for the beams. All the beams tested were simply-supported and under two-point loads, and a loading jack with a capacity of 100 tonnes was used to apply a concentrated load on a steel redistribution beam to generate the two concentrated loads.

The load applied on beams was initially about 5% of the ultimate load-carrying capacity of the beam (based on the theoretical calculation), and then increased step by step with a constant load increment for each step. In addition, a cycle of about 5% of the ultimate load was applied prior to the formal test in order to verify the good work performance of the mechanical and electronic equipments. After each load increment, a minimum lasting time of three minutes was required to ensure that the deformation of

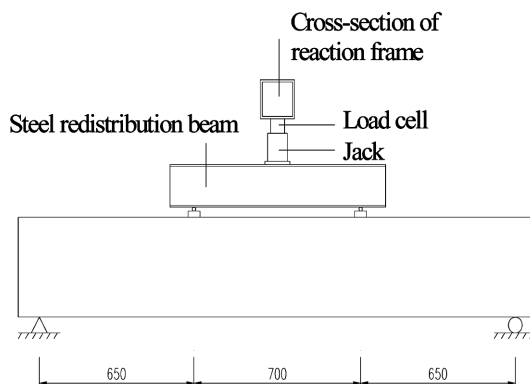


Fig. 6 Test setup

the beam would not change any longer. Continue to load until the beam ended up in failure.

### 3. Summary of test results

#### 3.1 Failure process and modes

As the applied load increased, the noise of the separation between side steel plates and the encased masonry as well as the cracking sound of the compression masonry, could be heard in the initial stage of loading. Then, the side steel plates between the binding bolts located in the top compression zone began to separate from the masonry (Fig. 7). After that, slight local buckling emerged outwards on the side steel plates. Finally, the side steel plates exhibited apparent local buckling (Fig. 8), accompanied by masonry crushing. Moreover, since beam L1 had no bottom plate, the encased masonry even glided downward from the external side steel plates (Fig. 9). Table 3 shows the percentage of each applied load corresponding to the specific phenomena mentioned above.

In order to obtain more information about the failure modes, all the damaged masonry was further observed after removing the external steel plates. The failure modes are described in detail as follows.

Fig. 10 shows the damage of the encased masonry in beam L1. Some wide cracks were found in the



Fig. 7 Separation between steel plate and masonry

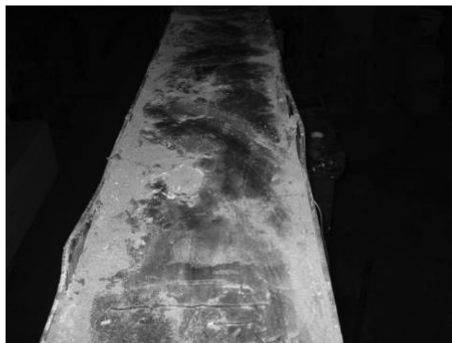


Fig. 8 Local buckling of steel plates in the compression zone of beams



Fig. 9 Encased masonry gliding downward

Table 3 Percentages of applied loads corresponding to the failure phenomena

Beam	Separation between steel plate and encased masonry	Slight local buckling of steel plate	Apparent local buckling of steel plate
L1	78%	90%	97%
L2	67%	89%	96%
L3	72%	85%	94%
L4	75%	87%	94%

masonry located in the compression zone of the beam. In addition, the encased masonry lost its integrity and could be separated easily when it was overturned.

In beam L2, longitudinal cracks were seldom observed in the encased masonry. Compared with beam L1, the integrity of the encased masonry in beam L2 was improved, because the injection cement grout filling the gaps within the component bricks strengthened their connection.

In beam L3, the injection epoxy adhesive exhibited a better bonding effect than that of cement grout; thus, the height of the local-buckling area of the side steel plate in beam L3 was lower than that in beam L2. As a result, the top masonry in the bending zone was not crushed, and both the side plates and the bottom plate were well bonded with the encased masonry, except that some steel plates experienced local buckling. Furthermore, the integrity of the encased masonry was relatively good, with only a few



Fig. 10 Damaged masonry of beam L1



Fig. 11 Masonry crushing in compression zone

Table 4 Ultimate loads of all tested beams

Beam	Ultimate load (kN)	Increase of ultimate load
L1	209	/
L2	356	70.3% compared with L1
L3	560	57.3% compared with L2
L4	630	12.5% compared with L3

tiny cracks appearing in the masonry located at the mid-span section.

The overall failure mode of beam L4 was similar to that of beam L3; the difference was that in beam L4, the masonry was crushed where the steel plates experienced local buckling, as shown in Fig. 11.

### 3.2 Ultimate capacity

The ultimate loads of all the tested beams are shown in Table 4, and the increase of ultimate load between two related beams is also provided.

### 3.3 Strain distribution of the steel plate along the beam depth

The strain distributions of the steel plates in the mid-span along the depth of beams L1, L2, L3, and L4 are plotted in Fig. 12. The strain distributions of the steel plates located at the loading points along the depth of beams L1 and L3 are also shown in Fig. 13, and the strain distributions in other beams have similar characteristics. Figs. 12 and 13 show that the strain distribution along the beam depth in the cross-section of the mid-span and the loading points was nearly linear before local buckling and the yielding of steel plate, verifying the assumption of plane section. Furthermore, this result is in accordance with the result of the field test by Jing *et al.* (2009).

### 3.4 Curve of load-deflection

Fig. 14 shows load-deflection curves at the mid-span for all the beams. According to the figure, the initial curves were nearly linear, followed by a temporary sharp increase of slope when the load reached 20% to 25% of the ultimate load. Such increase indicates an improvement in the flexural stiffness of the composite beam. This improvement is attributed to the gap elimination inside the masonry under the

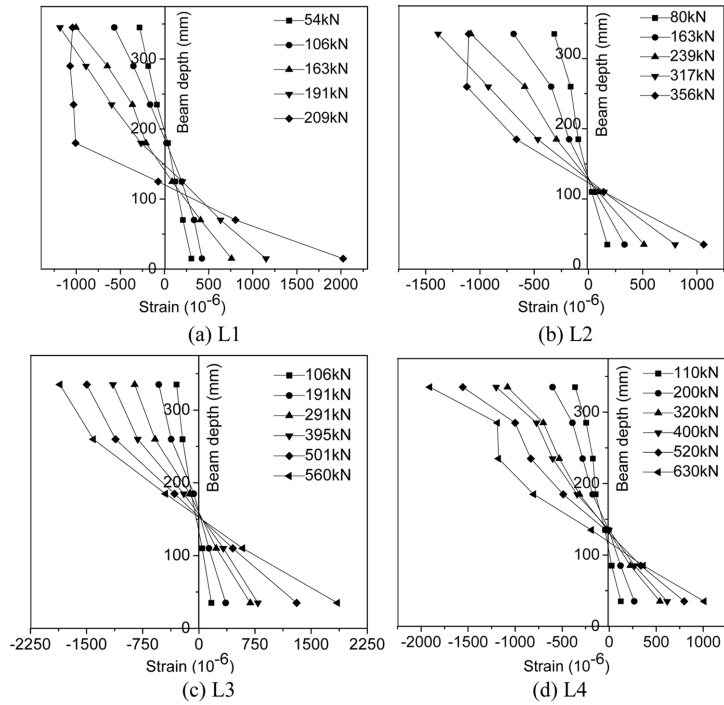


Fig. 12 Strain distributions at the location of mid-span

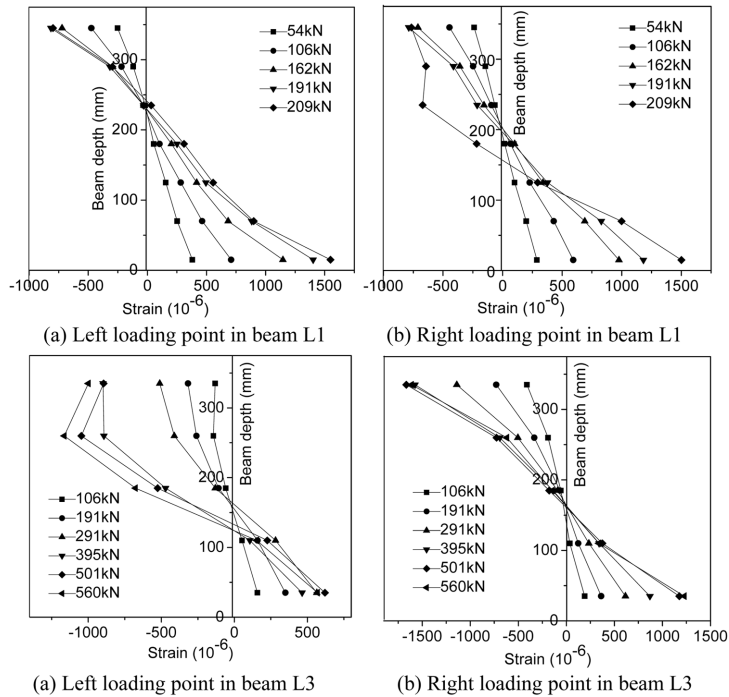


Fig. 13 Strain distributions at the locations of loading points

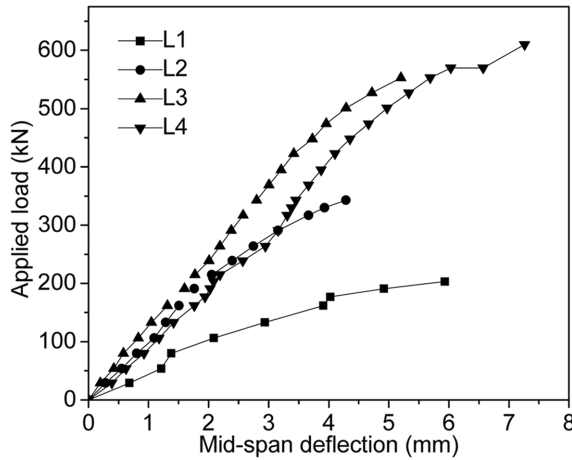


Fig. 14 Load versus mid-span deflection of all the beams

gradually increasing load. Afterwards, the curves became nearly linear again and then softened corresponding to the local buckling of the steel plate occurred. The curve eventually ended with the loss of load-carrying capacity.

### 3.5 Development of longitudinal strains at the top edge of side steel plates

Fig. 15 shows the change of average compressive strain readings at the top edge of side steel plates until separation started between the side steel plates and the encased masonry. It is clear in the figure that for beams L1, L2, and L3, steel plate strain increased linearly with the increase of load before the yielding strain is reached, and only the steel plate strain of beam L4 exceeded its yielding strain. Moreover, it can be noted that the slopes of the curves for beams L1 and L2 were similar, apparently smaller than those of beams L3 and L4 which were also very similar.

Fig. 16 shows the almost complete strain development of the steel plate in the compression zone of beams L2 and L3, indicating that each curve had an obvious inflection point. The figure also indicates

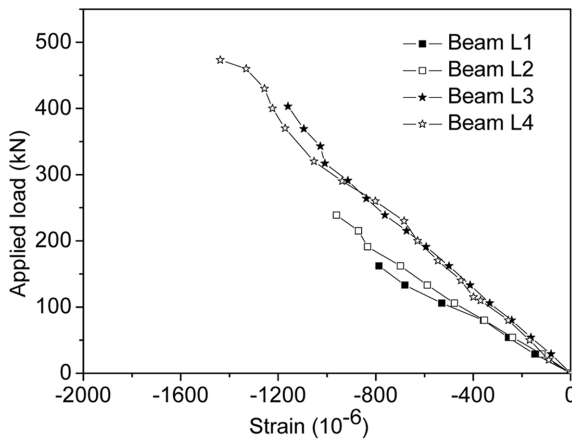


Fig. 15 Average strain at the top edge of side plate in each beam

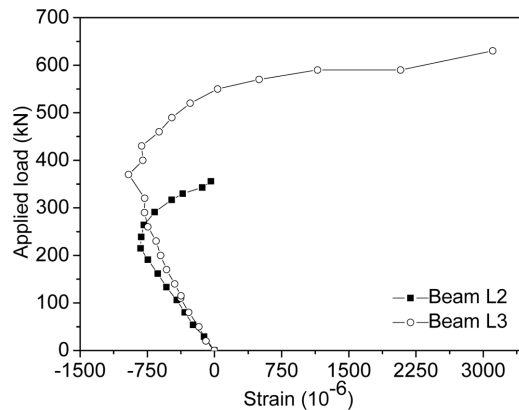


Fig. 16 Strain development of steel plate in the local buckling zone

that the loads corresponding to the inflection points in beams L2 and L3 were 225 kN and 375 kN, respectively.

## 4. Discussions of test results

### 4.1 Local buckling of steel plate

In the composite beams tested in the present study, steel plate is subjected to the constraints of binding bolts, encased masonry, and even the injection material. Therefore, the steel plate demonstrated unidirectional local buckling similar to those observed in concrete-filled thin-walled steel tubular beam-columns (Cai and He 2006, Cai and Long 2009, He *et al.* 2006, Liang *et al.* 2007). There exist obvious differences in the maximum average compressive strains (-0.000787, -0.000961, -0.001160, and -0.001438 for beams L1, L2, L3, and L4, respectively) at the top edge of side steel plates corresponding to their separation from the encased masonry (Fig. 15). The possible reasons for the above differences are explained as follows: (1) Beam L1 was not injected with any injection material, while beam L2 was injected with cement grout, which could fill the internal gaps between the steel plates and the encased masonry. With the gaps between the steel plates and the encased masonry, the steel plates are prone to bidirectional buckling rather than unidirectional buckling. It is well known that the critical stress of unidirectional buckling in thin plates is higher than that of bidirectional buckling (Siede 1958). (2) Beams L2 and L3 had the same dimensions yet different injection materials. The maximum average compressive strain of beam L3 increases by 22% compared with that of beam L2, which is mainly attributed to the influence of the greater lateral bonding stress of epoxy adhesive compared with that of cement grout. This also verifies that lateral bonding stress is an important factor affecting the local buckling of steel plates in this type of composite elements, and thus should not be ignored. (3) The bolt spacing was the same in these four beams, but beam L4 had 7.3 mm thick side plate different from 5.6 mm plate for the other three beams. In regard to the ratio of horizontal bolt spacing to steel plate thickness, the ratio for beam L4 is smaller than that for other beams by about 23%. Furthermore, the steel plate yielded in beam L4. Consequently, it can be said that both the ratio and the plate yielding help contribute to the larger average maximum compressive strain in beam L4.

In Fig. 16, the curves present clear inflection points, which can be regarded as the critical state of the local buckling of the steel plate. Therefore, the above-mentioned values, 225 kN and 375 kN, although relatively smaller, approach the loads corresponding to the moment when the steel plate separated from the encased masonry (239 kN and 403 kN, with only a little difference of 6.2% and 7.5%, respectively). Although the determination of buckling initiation is important, it is difficult to judge the initiation or exact buckling point once the post-buckling load-carrying capacity of the structure increases (Singer *et al.* 2002). In view of the relatively smaller difference, the load corresponding to the separation of steel plate from encased masonry can be regarded as the load when local buckling of the steel plate just started. Accordingly, the local buckling loads for beams L1, L2, L3, and L4 were 163, 239, 403, and 473 kN, respectively.

#### 4.2 Load-carrying capacity and influencing factors

Table 4 lists the ultimate load of each beam. The 70.3% increase in beam L2 compared with beam L1 is mainly ascribed to the addition of the bottom plate and the larger critical stress of side plate, which help increase the internal lever arm of the resisting moment. In addition, the loads at the local critical buckling of steel plate in beams L2 and L3 are larger than that in beam L1 by 47% and 147%, respectively. Hence, during the construction process, the load-carrying capacity of the composite beam without the bottom plate and the injection material is relatively low, so monitoring its safety is quite necessary. If regular monitoring is unavailable, reasonable safety supports must be supplied.

It can also be seen from Table 4 that a better the bonding strength of the injection material leads to a larger the ultimate load, although the increase in applied load is not infinite or linear. Beam L4 employed thicker plates (both the side plates and the bottom plate) compared with beam L3, and the increase in steel plate cross-sectional area is 39.9%, whereas the increase in its ultimate load is only 12.5%. The cause lies in the fact that when the steel plate in the compression zone experiences local buckling, part of its compressive force is transferred to the masonry, but the compressive strength of the masonry is very limited (see Table 2). That is to say, the ultimate load of a composite beam is mainly influenced by local buckling strength of steel plate rather than the strength of steel.

Besides, the spacing of the binding bolts is also a key parameter (He *et al.* 2006), but this is not considered in the present paper. For this reason, further investigation is needed.

Furthermore, according to the experimental data presented in Table 3, the steel plates in the composite beams began to separate from the encased masonry and experienced unilateral local buckling at the load level of about 67-78% of the ultimate load; after that, slight and apparent local buckling deformation occurred. In practical applications, slight and/or apparent local buckling deformation is not a preferred condition, especially in the service limit state. Therefore, based on the existing bolt spacing and the dimensions of the steel plate studied in this paper, the service load of steel plate-masonry composite beam is about 67-78% of the ultimate load.

#### 4.3 Flexural stiffness of composite beam

Fig. 14 shows that the maximum deflection of all the beams at ultimate limit state was 7.26 mm, and the corresponding deflection-to-span ratio was about 1:275. In addition, when the steel plate experienced critical local buckling, the deflection for all the beams was within 4.7 mm, indicating that the deflection-to-span ratio was about 1:426. During the application of steel plate-masonry composite structures, the local critical buckling stress of the steel plate serves as a main control parameter, i.e., the

design capacity is based on the limit state of the steel plate undergoing local buckling. The ultimate strength corresponding to the post-buckling of the steel plate cannot be used in the service limit state, but can be taken as a reserve strength for extra ultimate states, such as in earthquakes. According to the code for concrete structure designs in China (GB 50010, 2002), the minimum allowable deflection is around 1/400 of the clear span for flexural members. As a result, compared with reinforced concrete beams, steel plate-masonry composite beams have reasonable flexural stiffness, meeting the requirements for flexural members in practical applications.

#### 4.4 Contribution of encased masonry to flexural capacity of beam

From Table 2, compressive strengths of the encased masonry injected with cement grout and epoxy adhesive were 2.13 MPa and 3.13 MPa, respectively. In order to measure the contribution of encased masonry to the flexural capacity of composite beam, it is necessary to compare the resisting moment  $M_e$  (assumed by steel plates according to the assumption of plane section and strains of the mid-span cross-section in the experiment), with  $M_a$ (calculated from applied loads). Considering the design-oriented requirement and the accuracy of analysis, only the states within elastic local buckling of steel plate in composite section are adopted. In other words, values of loads on beam L4 are ruled out, since the local critical buckling stress of the steel plate exceeded its yielding strength. Detailed calculating process of  $M_e$  and  $M_a$  is described in Equations (1) and (2), where  $y$  is the distance from the top edge of side steel plate to the neutral axis of the steel plate composite section,  $E$  is the elastic modulus of steel,  $I$  is the moment of inertia of steel plate composite section,  $\varepsilon$  is the strain of side steel plate,  $F$  is the applied load, and  $l_1$  is the shear span length equal to 0.65 m.

$$\varepsilon = \frac{M_e \times y}{E \times I} \quad (1)$$

$$M_a = \frac{F \times l_1}{2} \quad (2)$$

The comparison results are tabulated in Table 5, and it indicates that when the beam is not injected with epoxy adhesive (e.g., beams L1 and L2), the difference between  $M_e$  and  $M_a$  is relatively small, i.e., the contribution of the encased masonry can generally be disregarded. However, when the beam is injected with epoxy adhesive (e.g., beam L3), the difference is relatively significant, i.e., the contribution of masonry should not be neglected, although the compressive strength of the masonry is much lower than that of the steel plate.

When the epoxy adhesive is injected, the integrity and the strength of the encased masonry are also improved due to the penetration of epoxy. At this moment, the internal masonry aids the external steel plates to resist larger compressive force, enhancing the internal lever arm of composite cross-section.

Table 5 Comparison of flexural capacities of beams

Beam	$\varepsilon$ ( $10^{-6}$ )	$y$ (mm)	$M_e$ (kN·m)	$M_a$ (kN·m)	$M_e / M_a$
L1	-1003	169	49.8	53.0	0.94
L2	-1083	200.5	79.7	77.7	1.03
L3	-1146	200.8	84.4	131.0	0.64

## 5. Conclusions

In this paper, steel plate-masonry composite structure is first introduced, followed by detailed description and discussions of the experimental results on the flexural behaviours of four steel plate-masonry composite beams. From the test data, discussions and analyses presented in this paper, the following conclusions can be drawn.

1. Failure of steel plate-masonry composite beams always starts from the local buckling of the steel plate located in the compression zone produced by bending moment, usually accompanied by masonry damage in the ultimate state. The local buckling of the steel plate in this type of composite beam with injection material is unidirectional in nature. Furthermore, during the construction process of this type of composite beam, the load-carrying capacity of the beam is considerably limited when the beam has neither bottom plate nor injection material. Therefore, it is essential to fully monitor the construction process of the composite beams, or reasonable safety supports must be supplied.

2. The assumption of plane section is acceptable in steel plate, which has not yielded or separated from the encased masonry in the steel plate-masonry composite beam.

3. Lateral bonding stress of epoxy adhesive is an important factor affecting the local buckling of steel plates, since it effectively increases the local critical buckling stress and thus increases the ultimate load of the composite beam. For the given conditions in this paper, the average critical stress of the steel plate in the beam injected with the epoxy adhesive increases by 22% compared with that in the beam with cement grout. As a result, the effect on lateral bonding stress from epoxy adhesive should be considered when designing steel plate-masonry composite beams.

4. In terms of the service limit state, the service load of steel plate-masonry composite beam varies from 67% to 78% of the ultimate load.

5. The load-carrying capacity of this type of composite beam increases along with the increment of steel plate thickness, while the increment is nonlinear considering the effect of the local buckling of the steel plate.

6. The flexural stiffness of steel plate-masonry composite beam corresponding to critical local buckling of steel plate is relatively large, indicating that it can be applied in the service limit state.

7. The contribution of encased masonry to the flexural capacity of a composite beam depends on the injection material, such as epoxy adhesive. It is advisable to consider the beneficial effects of such injection material with high bonding behaviour. Nevertheless, if the injection material has a low bonding property, such as cement grout, then its contribution is insignificant.

## Acknowledgement

This work is supported by the National Science Foundation of China (NSFC) (Project No. 51008070) and the Priority Academic Program Development of Jiangsu Higher Education Institutions. The support is gratefully acknowledged.

## References

Borri, A., Casadei, P., Castori, G., and Hammond, J. (2009), "Strengthening of brick masonry arches with externally bonded steel reinforced composites," *J. Compos. Constr., ASCE*, **13**(6), 468-475.

- Cai, J. and He, Z.Q. (2006), "Axial load behavior of square CFT stub column with binding bars," *J. Constr. Steel Res.*, **62**(5), 472-483.
- Cai, J. and Long, Y.L. (2009), "Local buckling of steel plates in rectangular CFT columns with binding bars," *J. Constr. Steel Res.*, **65**(4), 965-972.
- Ewing, B.D. and Kowalsky, J.K. (2004), "Compressive behavior of unconfined and confined clay brick masonry," *J. Struct. Eng., ASCE*, **130**(4), 650-661.
- Galano, L. and Gusella, V. (1998), "Reinforcement of masonry walls subjected to seismic loading using steel x-bracing," *J. Struct. Eng., ASCE*, **124**(8), 886-895.
- GB 50010. (2010). *Code for Design of Concrete Structures*. China Architecture & Building Press, Beijing.
- Hardy, S.J. and Al-Salka, M.A. (1995), "Composite action between steel lintels and masonry walls," *Struct. Eng. Rev.*, **7**(2), 75-82.
- Hardy, S.J. (2000), "Design of steel lintels supporting masonry walls", *Eng. Struct.*, **22**(6), 597-604.
- He, Z.Q., Cai, J. and Chen, X. (2006), "Investigation of behavior of square CFT stub columns with binding bars under axial loads", *Bldg. Struct.*, **36**(8), 49-53.
- Jing, D.H., Cao, S.Y. and Guo, H.Z. (2009), "Application of steel plate-masonry composite structure technology for underpinning of masonry walls", *China Civ. Eng. J.*, **42**(5), 55-60.
- Liang, Q.Q., Uy, B. and Liew, J. (2007), "Local buckling of steel plates in concrete-filled thin-walled steel tubular beam-columns", *J. Constr. Steel Res.*, **63**(3), 396-405.
- Moghaddam, H.A. (2004), "Lateral load behavior of masonry infilled steel frames with repair and retrofit", *J. Struct. Eng., ASCE*, **130**(1), 56-63.
- Perera, R., Gómez, S. and Alarcón, E. (2004), "Experimental and analytical study of masonry infill reinforced concrete frames retrofitted with steel braces", *J. Struct. Eng., ASCE*, **130**(12), 2032-2039.
- Siede, P. (1958), "Compressive buckling of a long simply supported plate on an elastic foundation", *J. Aero. Sci.*, **25**(3), 382-394.
- Singer, J., Arbocz, J. and Weller, T. (2002), *Buckling Experiments: Experimental methods in Buckling of Thin-Walled Structures: Shells, Built-Up Structures, Composites and Additional Topics*, John Wiley & Sons, New York.
- Taghdi, M., Bruneau, M. and Saatcioglu, M. (2000), "Seismic retrofitting of low-rise masonry and concrete walls using steel strips", *J. Struct. Eng., ASCE*, **126**(9), 1017-1025.